

# A PARALLEL PARTICLE-PARTICLE, PARTICLE-MESH SOLVER FOR STUDYING COULOMB COLLISIONS IN THE CODE IMPACT-T\*

Chad Mitchell<sup>†</sup> and Ji Qiang  
LBNL, Berkeley, CA 94720, USA

## Abstract

In intense charged-particle beams, the presence of Coulomb collisions can result in growth of the beam slice energy spread and emittance that cannot be captured correctly using traditional particle-in-cell codes. Particle-particle, particle-mesh solvers take a hybrid approach, combining features of N-body and particle-in-cell solvers, to correctly capture the effect of short-range particle interactions with less computing time than direct N-body solvers. We describe the implementation and benchmarking of such a solver in the code IMPACT-T for beam dynamics applications.

## INTRODUCTION

Coulomb collisions can play a significant role in the dynamics of low emittance, high-intensity beams for applications such as high-brightness photoinjectors, electron microscopy, and storage ring light sources [1, 2]. Short-range fluctuations in the fields seen by each particle can result in a growth of emittance and energy spread that is not captured by traditional accelerator particle-in-cell codes, which assume a smooth (mean-field) model of the beam space-charge seen by each particle.

These effects can be captured by N-body solvers that directly compute the Coulomb particle-particle interactions for every particle pair [3]. However, the successful use of these solvers is limited to beams with extremely low bunch charge, since computing times scale as  $O(N_p^2)$ , where  $N_p$  is the number of particles per bunch. In cosmology, plasma physics and molecular dynamics, such collisional many-body problems have been treated successfully [4, 5] using particle codes with improved scaling ( $O(N_p \log N_p)$  or better) including tree codes [6] and particle-particle, particle-mesh ( $P^3M$ ) solvers [7]. The application of these methods to charged-particle beams is relatively new in the context of accelerator systems. In this paper, we describe the implementation of a parallel  $P^3M$  solver in the photoinjector code IMPACT-T [8].

## THE $P^3M$ SOLVER

The solver is based on the algorithm described in Chapter 8 of [7]. In the reference frame in which the bunch centroid is at rest, the Coulomb force on a particle at location  $\mathbf{x}_i$  due to a particle at location  $\mathbf{x}_j$  is expressed in terms of the displacement  $\mathbf{r}_{ij} = \mathbf{x}_i - \mathbf{x}_j$  as:

$$\mathbf{F}(\mathbf{r}_{ij}) = \frac{q^2 \mathbf{r}_{ij}}{4\pi\epsilon_0 |\mathbf{r}_{ij}|^3} = \mathbf{F}^S(\mathbf{r}_{ij}) + \mathbf{F}^L(\mathbf{r}_{ij}). \quad (1)$$

\* Work supported by the U.S. Department of Energy under Contract No. DE-AC02-05CH11231.

<sup>†</sup> Chad.Mitchell@lbl.gov

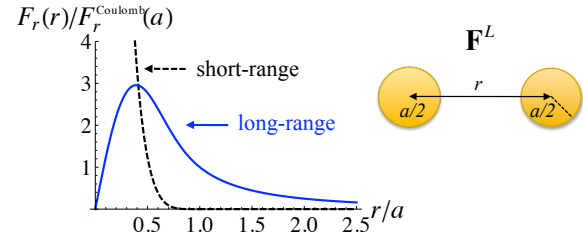


Figure 1: Short-range and long-range contributions to the Coulomb force between two particles (1) for a given cutoff radius  $a$  used by a  $P^3M$  solver in IMPACT-T.

Both  $\mathbf{F}^S$  and  $\mathbf{F}^L$  are radial forces determined by the inter-particle distance  $r = |\mathbf{r}_{ij}|$  and a parameter  $a$  known as the *cutoff radius*. The long-range contribution  $\mathbf{F}^L$  is the smooth, nonsingular force between two spherically-symmetric distributions of charge  $q$  and radius  $a/2$  whose centroids are separated by distance  $r$ , while the short-range contribution  $\mathbf{F}^S$  satisfies  $\mathbf{F}^S(r) = 0$  for  $r > a$ . See Figure 1. We use expressions for  $\mathbf{F}^S$  and  $\mathbf{F}^R$  corresponding to the S2 shape function described in (8-3) of [7].

The net long-range force acting on each particle is computed in the beam rest frame by solving on a mesh for the long-range contribution to the corresponding electric and magnetic fields. This is done using an FFT-based convolution procedure [7, 8]. The net short-range force acting on each particle is computed in the beam rest frame by directly summing the short-range forces due to all other particles in the beam. To reduce computing time, in addition to the potential mesh, a second *chaining cell* mesh is introduced whose cells have side  $HC \geq a$ . At each timestep, particles are sorted according to chaining cell location. During the short-range force computation, the solver needs to sum only over the subset of particles that lie within the current chaining cell or its nearest neighbors. The long-range and short-range force computations are each parallelized using domain decomposition [4, 5].

The cutoff radius  $a$  is typically chosen as 3-4 times the side  $H$  of a potential mesh cell. In the limit  $a \rightarrow 0$  for fixed  $H$ , one has  $\mathbf{F}^S \rightarrow 0$  and the  $P^3M$  computation is equivalent to a particle-in-cell computation (approximating a mean-field model), while in the limit  $a \rightarrow \infty$  for fixed  $H$ , one has  $\mathbf{F}^L \rightarrow 0$  and the  $P^3M$  computation is equivalent to a direct N-body simulation (all collisional effects are included).

## BENCHMARKS

### Expansion of a cold Spherical Beam

For this benchmark, we investigate a 0.25 nC electron bunch with a kinetic energy of 250 MeV undergoing free-space Coulomb expansion in a drift. The initial spatial distribution of particles is taken to be uniform within an ellipsoid with semi-principal axes  $a_x = a_y = \gamma a_z = R_0$ , which corresponds to a uniformly-charged sphere of radius  $R_0 = 1$  mm in the reference frame co-moving with the bunch centroid. The bunch is taken to have zero initial momentum spread.

In the bunch rest frame, the bunch is described as a uniformly-populated sphere of increasing radius:

$$R(t) = R_0 g(t/T), \quad (2a)$$

where  $g$  is the solution of the dimensionless envelope equation:

$$g'' = 1/g^2, \quad g(0) = 1, \quad g'(0) = 0, \quad (2b)$$

and the time scale  $T$  for space-charge expansion is given by:

$$T = \left( \frac{R_0^3}{N_p r_c c^2} \right)^{1/2} = \frac{\sqrt{3}}{2\pi} \tau. \quad (2c)$$

Here  $N_p$  is the bunch population,  $r_c$  is the classical particle radius, and  $\tau = 2\pi/\omega_p$  is the plasma period associated with the initial beam density.

Fig. 2 shows the evolution of the rms beam sizes along each dimension as computed by tracking a beam in IMPACT-T using the P<sup>3</sup>M solver described in the previous section. These results are shown together with the prediction  $\sigma_x = \sigma_y = \gamma\sigma_z = R(t)/\sqrt{5}$  obtained from (2). This simulation was performed using 10K particles with a  $64 \times 64 \times 64$  potential mesh and 2500 time steps. The cutoff radius was chosen by setting  $a = 3H$  at each timestep, where  $H = \max\{H_x, H_y, H_z\}$  denotes the size of a potential mesh cell. Because the evolution of RMS beam size is relatively insensitive to collisional effects, this is primarily a benchmark of particle tracking in the presence of the delicate cancellation between transverse forces due to electric and magnetic space-charge fields in the laboratory frame, that occurs for an intense relativistic beam.

While electron interactions with the linear space-charge fields within an expanding, uniformly-charged ellipsoid produce no emittance growth, some emittance growth is expected to occur due to Coulomb collisions. Fig. 3 shows the evolution of the rms beam emittance that is obtained using a direct N-body simulation including all Coulomb particle-particle interactions among the 10K simulation particles (black). This emittance growth is enhanced relative to the physical beam, since the number of simulation particles is less than the true number of electrons. However, Fig. 3 also shows the emittance growth obtained using the P<sup>3</sup>M solver for several values of cutoff radius. This emittance converges to the emittance obtained using the direct N-body simulation as the parameter  $a$  increases, indicating that the

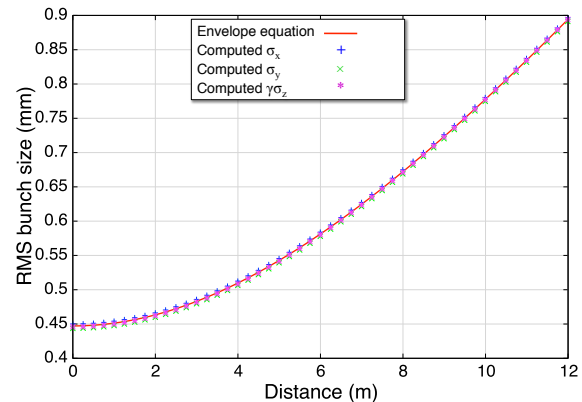


Figure 2: RMS beam sizes  $\sigma_x$ ,  $\sigma_y$ , and  $\gamma\sigma_z$  as functions of drift distance for a 0.25 nC electron bunch expanding in free space at 250 MeV, for comparison with (2). Results are obtained using a P<sup>3</sup>M solver with  $a/H = 3$ .

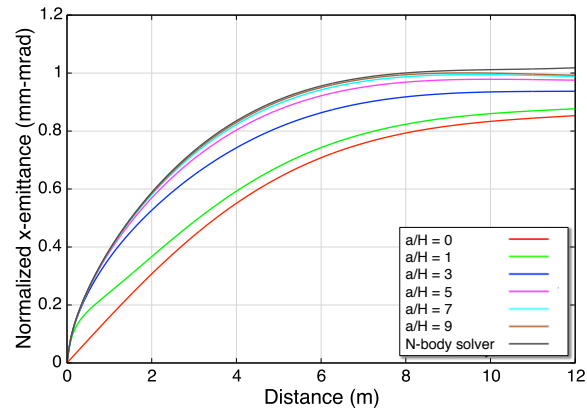


Figure 3: RMS horizontal emittance of a 0.25 nC electron bunch expanding in free space at 250 MeV as obtained using a particle-in-cell solver (red), a direct N-body solver (black), and a P<sup>3</sup>M solver with cutoff radii  $a/H = 1, 3, 5, 7$ , and  $9$ .

P<sup>3</sup>M solver correctly captures beam heating due to particle-particle collisions when the parameter  $a/H$  is sufficiently large.

### Disorder-induced Heating

For this benchmark, we investigate a 25 fC spherical electron bunch with zero initial momentum spread, whose particle coordinates have been initialized randomly within a sphere of radius  $R$ . The bunch is at rest and confined radially by using an applied linear focusing force that is equal and opposite to the repulsive force caused by the mean space-charge field. After a time of one-quarter plasma period, the initial disorder associated with the particles' coordinates is converted into disorder associated with the particles' momenta, through a collisional process of disorder-induced heating. The beam approaches a final equilibrium temperature  $T_{eq}$  corresponding approximately to the plasma coupling param-

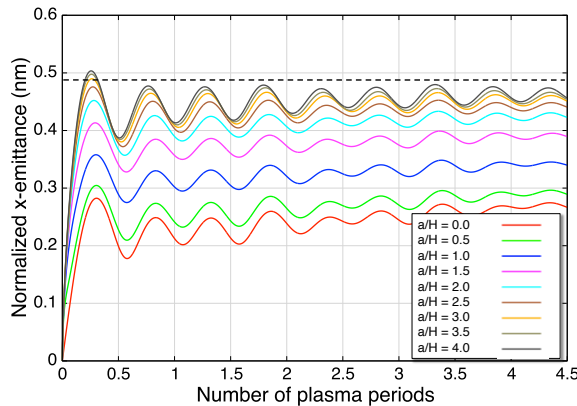


Figure 4: Emittance growth of a confined 25 fC electron bunch undergoing disorder-induced heating as obtained using a  $P^3M$  solver. Results are shown for several values of the cutoff radius  $a$ .

eter value [9]:

$$\Gamma_{\text{eq}} = \left( \frac{r_c}{d} \right) \left( \frac{mc^2}{k_B T_{\text{eq}}} \right) = 2.23, \quad (3)$$

where  $d$  is the Wigner-Seitz radius corresponding to the electron number density  $n_0$ :

$$d = \left( \frac{3}{4\pi n_0} \right)^{1/3}. \quad (4)$$

For a confined, spherical bunch of radius  $R$  consisting of  $N_p$  electrons, this gives an equilibrium temperature and rms emittance of:

$$\frac{k_B T_{\text{eq}}}{mc^2} = \frac{r_c N_p^{1/3}}{R \Gamma_{\text{eq}}}, \quad \epsilon_{x,n}^{\text{eq}} = \sigma_x \sqrt{\frac{k_B T_{\text{eq}}}{mc^2}}. \quad (5)$$

To simulate the disorder-induced heating process in IMPACT-T, we use a number of simulation particles equal to the true number of electrons  $N_p = 156055$ , which are confined within a sphere of radius  $R = 17.74 \mu\text{m}$  to produce a density of  $n_0 = 6.67 \times 10^{18} \text{ m}^{-3}$ . These parameters have been chosen to correspond to possible bunch charge and density near the cathode in a photoinjector used for ultrafast electron diffraction, as described in [10]. For the parameters given here  $k_B T_{\text{eq}} = 1.96 \text{ meV}$  and  $\epsilon_{x,n}^{\text{eq}} = 0.491 \text{ nm}$ .

Fig. 4 shows the simulated evolution of the rms beam emittance over 5 plasma periods. The result is shown for several values of the cutoff radius  $a$ , illustrating convergence to the predicted equilibrium value (dashed) as  $a/H$  increases beyond  $\sim 3$ . The oscillations of period  $\tau/2$  are characteristic of the disorder-induced heating process [9].

## SUMMARY

A parallel particle-particle, particle-mesh solver has been implemented in the code IMPACT-T for the purpose of studying collisional effects in high-brightness beams. While long-wavelength variations in the electric and magnetic self-fields are resolved on a computational mesh, the solver resolves the short-wavelength fluctuations in the electric and magnetic self-fields due to collisions by performing a direct summation of all particle-particle interaction forces within a given cutoff radius  $a$ . The accuracy of this procedure is primarily determined by the ratio  $a/H$ , where  $H$  is the size of a (potential) mesh cell, and benchmarks indicate that the emittance growth due to beam heating can be resolved when  $a/H \sim 3-7$ . In the presence of a photocathode, the  $P^3M$  solver also includes collision effects due to particle interactions with image charges at the cathode. Its application to simulations of a high-brightness photoinjector is underway.

## ACKNOWLEDGEMENT

This work is supported by the Office of Science of the U.S. Department of Energy under Contract No. DE-AC02-05CH11231 and made use of computer resources at the National Energy Research Scientific Computing Center.

## REFERENCES

- [1] A. Piwinski, Proc. 9th Intl. Conf. on High Energy Accel., Stanford, CA (1974); J. Borken and S. Mttingwa, Part. Accel. **13**, 115 (1983).
- [2] M. Reiser, *Theory and Design of Charged Particle Beams*, 2nd ed., Wiley-VCH, Weinheim, Germany (2008).
- [3] J. Qiang et al., "Numerical Study of Coulomb Scattering Effects on Electron Beam from a Nano-Tip," in Proceedings PAC'07, Albuquerque, NM, USA (2007).
- [4] T. MacFarland et al, *New Astronomy* **3**, 687-705 (1998).
- [5] R. J. Thacker and H. P. Couchman, "A Parallel Adaptive  $P^3M$  Code with Hierarchical Particle Reordering," *Computer Physics Communications*, **174**, 540 (2006).
- [6] J. Barnes and P. Hut, *Nature* **324**, 446-449 (1986); *Many Body Tree Methods in Physics* (1997).
- [7] R. W. Hockney and J. W. Eastwood, *Computer Simulation Using Particles*, McGraw-Hill, Inc., New York (1981).
- [8] J. Qiang, S. Lidia, and R. Ryne, *Phys. Rev. ST - Accel. Beams* **9**, 044204 (2006).
- [9] J. M. Maxson et al., "Fundamental photoemission brightness limit from disorder induced heating," *New Journal of Physics*, **15**, 103024 (2013).
- [10] D. Filippetto et al., "High Repetition Rate Ultrafast Electron Diffraction at LBNL", IPAC 2014, Dresden, Germany, June 2014, MOPRI053 (2014), <http://www.JACoW.org>